

## Accepted Manuscript

Strong-coupling induced damping of spin-echo modulations in magic-angle-spinning NMR: implications for  $J$  coupling measurements in disordered solids

Paul Guerry, Steven P. Brown, Mark E. Smith

PII: S1090-7807(17)30203-3

DOI: <http://dx.doi.org/10.1016/j.jmr.2017.08.006>

Reference: YJMRE 6145

To appear in: *Journal of Magnetic Resonance*

Received Date: 20 May 2017

Revised Date: 11 August 2017

Accepted Date: 17 August 2017

Please cite this article as: P. Guerry, S.P. Brown, M.E. Smith, Strong-coupling induced damping of spin-echo modulations in magic-angle-spinning NMR: implications for  $J$  coupling measurements in disordered solids, *Journal of Magnetic Resonance* (2017), doi: <http://dx.doi.org/10.1016/j.jmr.2017.08.006>

This is a PDF file of an unedited manuscript that has been accepted for publication. As a service to our customers we are providing this early version of the manuscript. The manuscript will undergo copyediting, typesetting, and review of the resulting proof before it is published in its final form. Please note that during the production process errors may be discovered which could affect the content, and all legal disclaimers that apply to the journal pertain.



# Strong-coupling induced damping of spin-echo modulations in magic-angle-spinning NMR: implications for $J$ coupling measurements in disordered solids

Paul Guerry<sup>a,b</sup>, Steven P. Brown<sup>b</sup> and Mark E. Smith<sup>\*b,c</sup>

<sup>a</sup>*Green Grow Scientific, 21 Montée de l'Observance, 69009 Lyon, France*

<sup>b</sup>*Department of Physics, University of Warwick, Coventry, CV4 7AL, UK*

<sup>c</sup>*Vice-Chancellor's Office, University House, Lancaster University, Lancaster, LA1 4YW, UK and Department of Chemistry, Lancaster University, Lancaster, LA1 4YB, UK*

\* Corresponding author at: Vice-Chancellor's Office, University House, Lancaster, LA1 4YW, UK

*E-mail address:* [m.e.smith@lancaster.ac.uk](mailto:m.e.smith@lancaster.ac.uk)

## ABSTRACT

In the context of improving  $J$  coupling measurements in disordered solids, strong coupling effects have been investigated in the spin-echo and refocused INADEQUATE spin-echo (REINE) modulations of three- and four-spin systems under magic-angle spinning (MAS), using density matrix simulations and solid-state NMR experiments on a cadmium phosphate glass. Analytical models are developed for the different modulation regimes, which are shown to be distinguishable in practice using Akaike's information criterion. REINE modulations are shown to be free of the damping that occurs for spin-echo modulations when the observed spin has the same isotropic chemical shift as its neighbour. Damping also occurs when the observed spin is bonded to a strongly-coupled pair. For mid-chain units, the presence of both direct and relayed damping makes both REINE and spin-echo modulations impossible to interpret quantitatively. We nonetheless outline how a qualitative

comparison of the modulation curves can provide valuable information on disordered networks, possibly also pertaining to dynamic effects therein.

Keywords strong  $J$  coupling, spin-echo modulation, phosphate glasses, experimental simulation

## 1. Introduction

$J$  couplings manifest themselves through their splitting of spectral lineshapes or via the modulation they impart to spin-echo signal intensities. It is well known that under strong coupling, additional peaks known as “strong-coupling artefacts” can appear in NMR spectra [1–3]. While strong coupling effects are often encountered in solution NMR spectroscopy [4], in solids, the presence of much stronger anisotropic interactions makes them irrelevant in most cases. However, recent developments for solid-state magic-angle spinning (MAS) NMR [5] may soon render this distinction obsolete.

The interest in  $J$  couplings here lies in the information they provide on networks in disordered systems such as phosphate glasses [6,7]. We have previously shown how couplings two orders of magnitude weaker than the linewidth in the direct dimension can be measured using the refocused INADEQUATE spin-echo (REINE) sequence [8]. In these systems, the broad distribution of isotropic shifts suggests that a substantial proportion of atom pairs are strongly coupled. Although the spin-echo [9] and refocused INADEQUATE [10,11] experiments (Fig. S1) have been shown to be robust in the presence of anisotropic interactions under MAS, complications are known to arise at rotational resonance, particularly  $n = 0$  rotational resonance (i.e. under strong coupling). Knowing whether the values measured experimentally are reliable or not is crucial if better structural models [12] or prediction methods [13] are to be developed.

This study builds on previous investigations of the spin-echo [9,14–16] and refocused INADEQUATE experiments [11] – the REINE experiment combines these two sequences. However, while these existing studies of the spin-echo experiment in the solid state consider two-spin systems only, we extend this analysis using density matrix simulations to three- and four-spin systems with two or more spins strongly

coupled. We also highlight important differences between REINE and spin-echo modulations. The predicted effects are investigated experimentally on a cadmium phosphate glass. Note that the experimental data considered in this study are the same as those presented in Ref. [8]; the focus here is on the new data analysis.

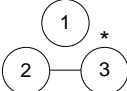
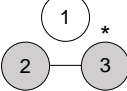
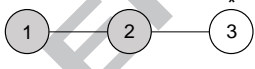
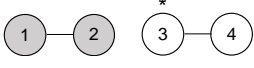
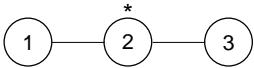
## 2. Methods

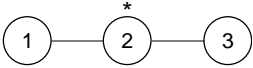
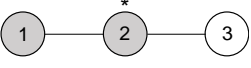
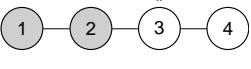
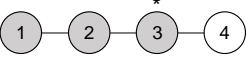
### 2.1. Simulations

Numerical simulations of the spin-echo and REINE experiments (Fig. 1) were performed using SIMPSON 4.1.1. [17], for up to 51 4 ms increments of  $\tau_j$ :  $\tau_j^{\max} = 0$  ms for comparisons of integrated intensities,  $\tau_j^{\max} = 40$  ms for comparisons under experimentally realistic conditions, and  $\tau_j^{\max} = 200$  ms to characterize the underlying effects. Representative SIMPSON input and data files are available through the Lancaster University repository [dataset 18].

The parameters used for the main set of calculations are presented in Table 1. These were chosen to reproduce the experimental data for the cadmium phosphate glass as closely as possible. In terms of the phosphate chain structure, spin systems spinsys1 and spinsys2 (Table 1) represent  $P_1$  pairs (in this notation, the subscript indicates the number of other  $^{31}\text{P}$  atoms each one is  $J$  coupled to), spinsys3 and spinsys4,  $P_1$  units at the end of a linear chain and spinsys5–8  $P_2$  units in chains of different lengths. (Note that it does not affect the analysis that the values of individual chemical shifts in some of these simulated spin systems do not correspond to the values for  $P_1$  and  $P_2$  units in the experimental example considered in this paper.) The difference in isotropic chemical shift,  $\Delta\delta_{\text{iso}}$ , between the observed spin (defined by the detect operator) and its strongly coupled neighbour(s) (nearest and/or next nearest neighbour) was varied from 0 to 4 ppm. The external magnetic field strength and MAS frequency were 7.05 T and 12.5 kHz, respectively. The dipole-dipole coupling between directly bonded phosphate units was set to between  $-670$  and  $-680$  Hz, in keeping with the P–O–P bond distances and angles reported in the literature [19–21]. Next-nearest neighbours were assumed to be  $\sim 4.4$  Å away (i.e. a coupling of about  $-230$  Hz) as in the crystal structure of  $\text{TiP}_2\text{O}_7$  [22], and when a fourth spin was simulated, this was assumed to be  $\sim 6.3$  Å away from the first.

TABLE 1.  $^{31}\text{P}$  NMR parameters of the physical systems simulated in this study.

Spin system <sup>a</sup>	Nucleus [pair]	$\delta_{\text{iso}}$ (ppm)	$\delta_{\text{CSA}}$ (ppm) <sup>a</sup>	$J$ (Hz)	$\mathbf{b}_{jk}/2\pi^b$ (Hz)
spinsys1 	1 [1, 3]	−16.0	65.0	−	−231
	2 [1, 2]	−30.0	61.5	−	−225
	3 [2, 3]	−34.0	61.5	21.5	−680
spinsys2 <sup>c</sup> 	1 [1, 3]	−16.0	65.0	−	−231
	2 [1, 2]	−30.0	61.5	−	−225
	3 [2, 3]	−30.0	61.5	21.5	−680
spinsys3 <sup>c</sup> 	1 [1, 2]	−30.0 <sup>c</sup>	61.5	21.5	−680
	2 [2, 3]	−30.0	61.5	15.5	−672
	3 [1, 3]	−16.0	65.0	−	−231
spinsys4 	1 [1, 2]	−30.0	61.5	21.5	−680
	3 [3, 4]	−14.0			−675
	2 [2, 3]	−30.0	61.5	−	−672
	4 [1, 3] [2, 4]	−12.0	65.0	−	−231
	[1, 4]	−	−	−	−81
spinsys5 	1 [1, 2]	−34.0	140.0	21.5	−680
	2 [2, 3]	−30.0	140.0	15.5	−672

		3 [1, 3]	−16.0	65.0	−	−231
	spinsys6	1 [1, 2]	−30.0	140.0	21.5	−680
		2 [2, 3]	−30.0	140.0	15.5	−672
		3 [1, 3]	−16.0	65.0	−	−231
	spinsys7	1 [1, 2]	−30.0	140.0	21.5	−680
		2 [2, 3]				
		3 [3, 4]	−14.0	140.0	15.5	−672
		4 [1, 3] [2, 4]	−12.0	65.0	−	−231
	spinsys8	1 [1, 2]	−30.0	140.0	21.5	−680
		2 [2, 3]				
		3 [3, 4]	−14.0	140.0	15.5	−672
		4 [1, 3] [1, 4]	−12.0	65.0	−	−231
		[1, 4]	−	−	−	−81

The shaded circles represent strongly-coupled spins. The asterisks indicate the detect operator for each spin system. The Euler angles for the chemical shift anisotropy (CSA) tensors and the internuclear vectors are shown in the example SIMPSON files available through the Lancaster University repository [dataset 18].

<sup>a</sup>Within a given spin system, the chemical shift tensors (with  $\eta = 0.20$  or  $0.15$  as in Ref. [11]) all have different principal components. The absolute values of the chemical shifts are irrelevant for this analysis: only the *differences* in isotropic chemical shift within each spin system are important, i.e., it does not affect the analysis that a value of  $-30$  ppm corresponds to a  $P_2$  not a  $P_1$  site in the experimental spectrum considered in this paper.

<sup>b</sup> $b_{jk} = -\frac{\mu_0}{4\pi} \frac{\gamma_j \gamma_k \hbar}{r_{jk}^3}$ , where  $\gamma_j$  and  $\gamma_k$  are the gyromagnetic ratios of the two spins, and  $r_{jk}$  the distance between them;  $\mu_0$  and  $\hbar$  are the magnetic and Planck's constant, respectively.

<sup>c</sup>Simulations with spinsys2 and spinsys3 were repeated with  $\Delta\delta_{iso}^{1,2}$  equal to the magic angle spinning frequency (12.5 kHz), i.e. with  $\delta_1^{iso} = -107.16$  ppm.

Strong coupling effects were also investigated over a wide range of MAS frequencies (5–100 kHz), dipole-dipole coupling strengths (phosphate glass values  $\times$

0.2–6.5) and chemical shift anisotropies (CSAs) (20–240 ppm), with each of these parameters systematically varied in turn for specific spin systems.

## 2.2. Sample preparation

A cadmium phosphate glass (starting composition  $0.575\text{CdO}-0.425\text{P}_2\text{O}_5$ ) was prepared as described by Hussin et al. [23]

## 2.3. NMR experiments

The spin-echo and REINE MAS NMR experiments performed on the cadmium phosphate glass have been described elsewhere [8], where the experimental data was originally presented. Briefly though, the experiments were performed at a  $^{31}\text{P}$  Larmor frequency of 121.5 MHz (external magnetic field, 7.05 T) and at 12.5 kHz MAS. The pulse sequences are shown in Fig. S1. A representative spin-echo spectrum and a REINE spectrum obtained with a modulating echo delay of 0 ms ( $\tau_j = 0$  ms) are shown in Fig. 1.

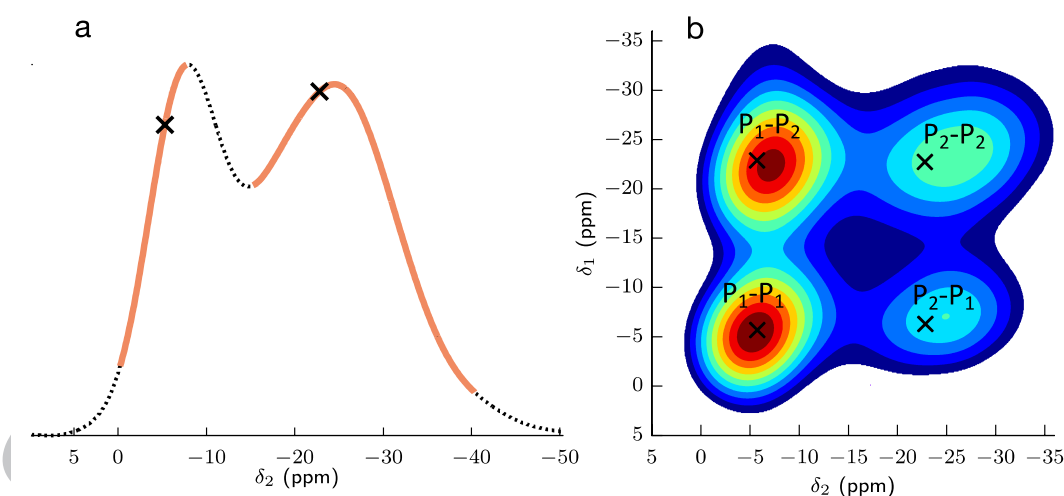


**Fig. 1.** Spin-echo and REINE (refocused INADEQUATE spin-echo) spectra recorded and presented as part of a previous study [8], showing the regions analysed in this work. (a) Spin-echo and (b) REINE  $^{31}\text{P}$  (121.5 MHz) magic-angle spinning (12.5 kHz) NMR spectra of a cadmium phosphate glass ( $0.575\text{CdO}-0.425\text{P}_2\text{O}_5$ ) recorded with a final ( $J$  modulating) spin-echo delay of 0 ms. The peaks are labelled in terms of their  $\text{P}_n$  assignment,  $n$  indicating the number of other  $^{31}\text{P}$  spins each one is  $J$  coupled to via a bridging oxygen. The thick solid orange lines in panel (a) correspond to the two regions of the spin-echo spectrum considered for fitting. The points marked with a cross are those whose echo modulation curves are shown in—clockwise from the left of panel (a)—Figs. 4a, 6a, 4b, 6b, 6c and 4c.

#### 2.4. Data fitting

The experimental and simulated  $J$  modulations (intensity versus  $\tau_j$ ) were fit using custom-written Python scripts [dataset 18]. The functions used are built around the standard equations for fitting spin-echo curves under the effects of one or two  $J$  couplings,

$$f_1 = \exp(-2\tau_j/T_2') \cdot \cos(2\pi J_1 \tau_j) \quad (1)$$

$$f_2 = \exp(-2\tau_j/T_2') \cdot \cos(2\pi J_1 \tau_j) \cdot \cos(2\pi J_2 \tau_j) \quad (2)$$

where  $T_2'$  is the spin-echo dephasing time [10] and the other symbols have their usual meaning. Duma et al. [9] have shown that at rotational resonance (notably at  $n=0$  rotational resonance, i.e. under strong coupling), spin-echo modulations are dampened by a zero-frequency term, whose relative amplitude depends on the MAS frequency, CSA and dipole-dipole coupling strength:

$$f_1^0 = p \cdot \exp(-2\tau_j/T_2') \cdot \cos(2\pi J_1 \tau_j) + (1 - p) \cdot \exp(-2\tau_j/T_2^0) \quad (3)$$

To avoid overfitting, approximate versions of the functions (denoted with a subscript “a”, with one or both decay times kept fixed) were used. This ensured that the ratio of data points to fitting variables was never less than 3.7 for the REINE data and 6 for the spin-echo data:

$$f_{1a}^0 = p \cdot \exp(-2\tau_j/T_2') \cdot \cos(2\pi J_1 \tau_j) + (1 - p) \cdot \exp(-2\tau_j/[0.5 \cdot T_2']) \quad (4)$$

$$f_{2a}^0 = p \cdot \exp(-2\tau_j/T_2'^{f_1}) \cdot \cos(2\pi J_1 \tau_j) + (1 - p) \cdot \exp(-2\tau_j/[0.5 \cdot T_2'^{f_1}]) \quad (5)$$

For  $f_{2a}^0$  (Eq. 5), the decay time  $T_2'^{f_1}$  was fixed to the value obtained by fitting single  $J$ -coupling modulations from the same dataset (with  $f_1$ ); the fitting parameters for



$f_{2a}^0$  are then  $p$ ,  $J_1$  and  $J_2$ . The decay of the experimental data was best fit using a mixed Gaussian-Lorentzian decay function,

$$\mathcal{K} = \exp \left[ (\Delta\tau_c)^2 \left[ -2\tau_j/T_2'^k + 1 - \exp(-2\tau_j/T_2'^k) \right] \right] \quad (6)$$

where  $\Delta$  represents the variance of the spectroscopic transition frequency and  $\tau_c$  is the relaxation time of the thermal bath [24,25]. A complete list of the fitting functions used in this study is provided in Table 2.

TABLE 2. Functions used to fit simulated and experimental spin-echo curves.

Functions used to fit simulated and experimental data	Fitting parameters	Fixed parameters
$f^0 = \mathcal{L}$	$T_2'$	—
$f_1 = \mathcal{L} \cdot C_1$	$J_1, T_2'$	—
$f_{1a}^0 = p \cdot \mathcal{L} \cdot C_1 + (1 - p) \cdot \mathcal{L}^0$	$J_1, T_2', p$	$T_2^0 = T_2'/2$
$f_2 = \mathcal{L} \cdot C_1 \cdot C_2$	$J_1, J_2, T_2'$	—
$f_{2a}^0 = p \cdot \mathcal{L} \cdot C_1 \cdot C_2 + (1 - p) \cdot \mathcal{L}^0$	$J_1, J_2, p$	$T_2' = T_2'^{f_1},$ $T_2^0 = T_2'/2$
Functions used to fit simulated data only		
$f_1^0 = p \cdot \mathcal{L} \cdot C_1 + (1 - p) \cdot \mathcal{L}^0$	$J_1, T_2', p, T_2^0$	—
$f_{1t} = \mathcal{L} \cdot [p \cdot C_1 + q \cdot C_{\Delta-} + (1 - p - q) \cdot C_{\Delta+}]$	$J_1, T_2', p, q$	—
$f_2^0 = p \cdot \mathcal{L} \cdot C_1 \cdot C_2 + (1 - p) \cdot \mathcal{L}^0$	$J_1, J_2, T_2', p, T_2^0$	—
Functions used to fit experimental data only		
$f^{0k} = \mathcal{K}$	$T_2'^k$	—
$f_1^k = \mathcal{K} \cdot C_1$	$J_1, T_2'^k$	—
$f_{1ak}^0 = p \cdot \mathcal{K} \cdot C_1 + (1 - p) \cdot \mathcal{L}^0$	$J_1, T_2'^k, p$	$T_2^0 = T_2'/2$
$f_{1ak}^{0k} = p \cdot \mathcal{K} \cdot C_1 + (1 - p) \cdot \mathcal{K}^0$	$J_1, T_2'^k, p$	$T_2^{0k} = T_2'^k/2$
$f_2^k = \mathcal{K} \cdot C_1 \cdot C_2$	$J_1, J_2, T_2'^k$	—

$$\begin{aligned}
 f_{2ak}^0 &= p \cdot \mathcal{K} \cdot C_1 \cdot C_2 + (1 - p) \cdot \mathcal{L}^0 & J_1, J_2, p & & T_2'^k &= T_2'^{kf_1}, \\
 & & & & T_2^0 &= T_2'^{f_1}/2 \\
 f_{2ak}^{0k} &= p \cdot \mathcal{K} \cdot C_1 \cdot C_2 + (1 - p) \cdot \mathcal{K}^0 & J_1, J_2, p & & T_2'^k &= T_2'^{kf_1}, \\
 & & & & T_2^0 &= T_2'^{f_1}/2
 \end{aligned}$$

Abbreviations:  $C_i = \cos(2\pi J_i \tau_j)$ ,  $J_{\Delta\pm} = J \pm (J^2 + \Delta\delta_{\text{iso}}^2)^{1/2}$

$\mathcal{K} = \exp[(\Delta\tau_c)^2[-2\tau_j/T_2'^k + 1 - \exp(-2\tau_j/T_2'^k)]]$ , with  $\Delta\tau_c = 1$ .

$\mathcal{K}^0 = \exp[-2\tau_j/T_2^{0k} + 1 - \exp(-2\tau_j/T_2^{0k})]$ ,

$\mathcal{L} = \exp(-2\tau_j/T_2^i)$ ,  $\mathcal{L}^0 = \exp(-2\tau_j/T_2^0)$

Each dataset was fitted with all potentially matching functions—those accounting for the appropriate number of  $J$  couplings—in turn, omitting those that would have overfitted the data. Akaike's information criterion was calculated for each model [26–28],

$$\text{AIC}_A = n_{\text{obs}} \cdot \ln \left[ \frac{\chi_A^2}{n_{\text{obs}}} \right] \cdot 2k_A + \frac{2k_A \cdot (k_A + 1)}{n_{\text{obs}} - k_A - 1} \quad (7)$$

(using the correction for small samples,  $\frac{2k_A \cdot (k_A + 1)}{n_{\text{obs}} - k_A - 1}$ ), where  $n_{\text{obs}}$  is the number of data points,  $k_A$ , the number of fitting parameters of model  $A$ , and  $\chi_A^2$  is the corresponding weighted sum of squared deviations:

$$\chi_A^2 = \sum_i \left[ \frac{\text{obs}_i - A_i}{\sigma_i} \right]^2 \quad (8)$$

In this study, each data point was assumed to have the same uncertainty,  $\sigma_i = \sigma = 0.02$ . The  $N$   $\text{AIC}_A$  (one  $\text{AIC}_A$  value for each model) values obtained were expressed as a difference from the minimum,

$$\Delta_A = \text{AIC}_A - \text{AIC}_{\text{min}} \quad (9)$$

and the best model was selected using the corresponding weight of evidence (WoE) [28],

$$\text{WoE}_A = \frac{\exp(-\Delta_A/2)}{\sum_{m=1}^N \exp(-\Delta_m/2)} \quad (10)$$

The advantages of Akaike's information criterion for model selection are that it allows models with different functional forms to be compared and avoids the arbitrary definition of a level of significance.

The data and model were also inspected in the frequency domain to make sure that the peak positions matched. The fit was considered successful if the corresponding  $\chi^2$  statistic (Eq 8) was of the same order of magnitude as the number of degrees of freedom (the number of free variables in the fitting function), df, i.e. if the reduced  $\chi^2$ ,  $\chi_{\text{red}}^2 = \chi^2/\text{df} \approx 1$ .

The experimental data were fit with no more than three free variables. For the spin-echo data, the regions considered for fitting are highlighted in Fig. 1.—the right-hand side of the  $P_1$  peak was omitted to avoid ambiguities due to peak overlap. For the REINE data (Fig. 1b), all points above a certain threshold of the local maximum (66% for the  $P_1$  peaks and 75% for the  $P_2$  peaks) in the spectrum at  $\tau_j = 0$  were considered. Results obtained over a whole peak are reported as the median value and the range between the 5<sup>th</sup> and 95<sup>th</sup> percentile (p5–p95).

### 3. Results

#### 3.1. End-of-chain units: simulations

Fig. 2 shows spin-echo and REINE intensity versus time curves obtained for spin systems spinsys1, spinsys2 and spinsys3 (Table 1).

In agreement with Duma et al., away from rotational resonance (Fig. 2a,b), only the ideal  $J$ -modulated component is observed, as confirmed by the high-resolution data (i.e., out to  $\tau_j^{\text{max}}/2 = 200$  ms) shown in Fig. S2a,b. At  $n = 0$  rotational resonance (Fig. 2c,d), the modulation of the spin-echo data is damped by a zero-frequency component (Fig. 2c and Fig. S2c; best fit functions,  $f_{1a}^0$  and  $f_1^0$ ,

respectively; WoE, 1.00), but the equivalent REINE data are not (Fig. 2d and Fig. S2d; best fit function,  $f_1$ ; WoE, 1.00). When the nearest neighbours of the observed spin are at rotational resonance (Fig. 2e,f and Fig. S2e,f), the spin-echo and REINE curves are both damped by a zero-frequency component (best fit functions  $f_{1a}^0$  and  $f_1^0$  for the low- and high-resolution data, respectively; WoE, 1.00). Note that even for the low-resolution data ( $\tau_j^{\max} = 40$  ms) and in all three situations, the fitting procedure unambiguously selects the appropriate function and the fitted values of the  $J$  coupling are accurate (within 4% of the simulated value).

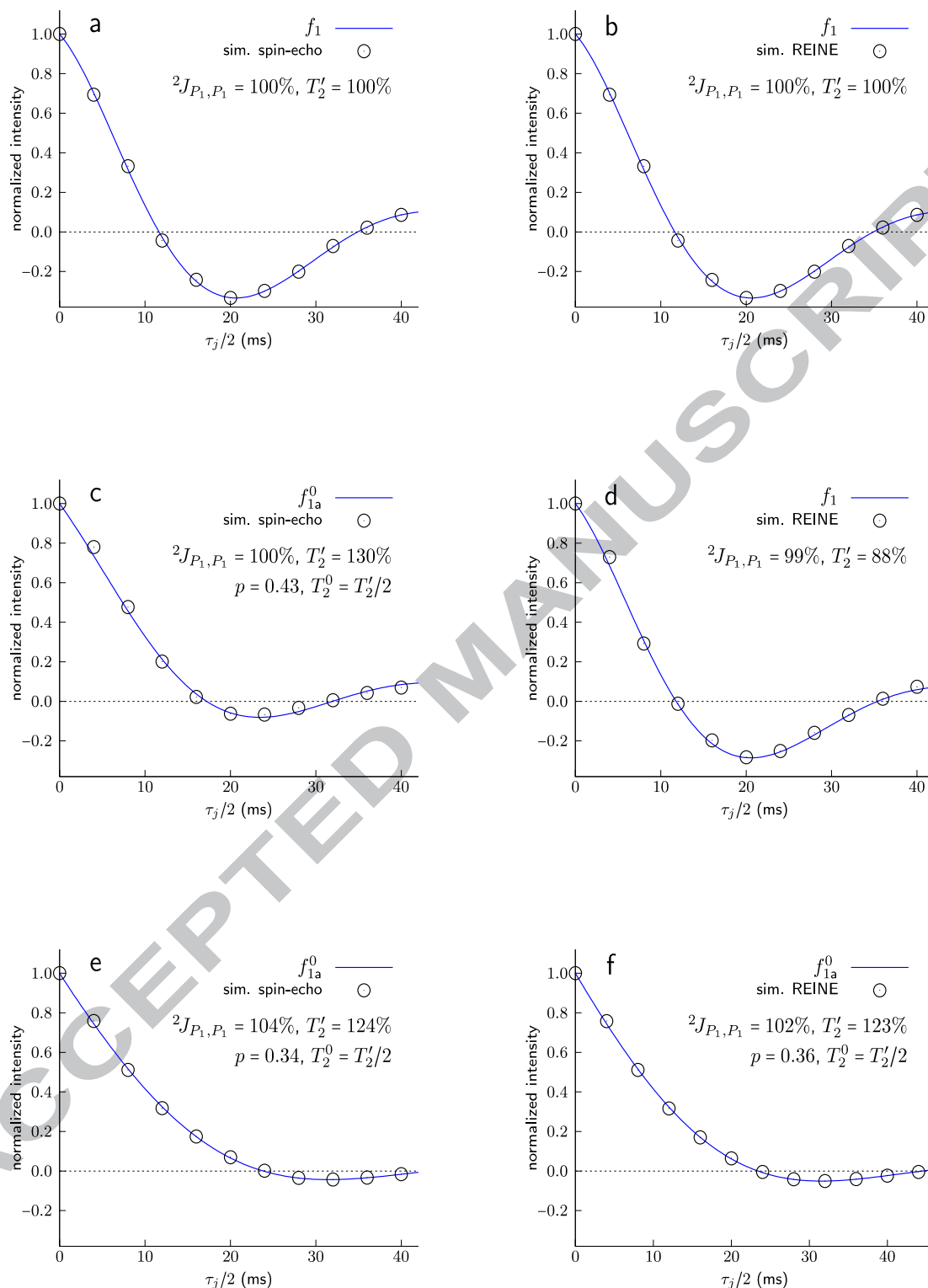


**Fig. 2.** Strong coupling effects in spin-echo and REINE curves from end-of-chain units. Simulated  $^{31}\text{P}$  (121.5 MHz) MAS (12.5 kHz) NMR (a, c, e) spin-echo and (b, d, f) REINE (refocused INADEQUATE spin-echo) intensities as a function of the modulating spin-echo delay ( $\tau_j$ ) of the third spin of three-spin systems with differences in isotropic chemical shift (a, b)  $\Delta\delta_{\text{iso}}^{2,3} = 4$  ppm (spinsys 1 in Table 1), (c, d)  $\Delta\delta_{\text{iso}}^{2,3} = 0.0$  ppm (spinsys2) (e, f)  $\Delta\delta_{\text{iso}}^{1,2} = 0.0$  ppm (spinsys3). The optimised fitting parameters (inset) are expressed as a percentage of the corresponding simulated value,  $J^{2,3} = 21.5$  (parts a–d) or 15.5 Hz (parts e,f), and  $T'_2 = 40$  ms.

Section 3 of the supporting material (Figs S3–9) shows that similar results are obtained for a wide range of MAS frequencies (5–100 kHz), dipole-dipole coupling strengths (–200 to –1600 Hz) and CSAs (40–280 ppm). (Note the caveat that each of these parameters was varied in turn rather than as part of a complete grid search). For the direct coupling effect, this roughly corresponds to regime B described by Duma et al. [9] (in section 2.4.7), for which their analysis also predicts damped spin-echo oscillations. However, the present results indicate in addition that the ideal  $J$  modulation is always more prominent in REINE than in spin-echo data. The relayed damping effect seems to be parameter independent and affects both experiments in the same way.

The normalised scales in Fig. 2 ( $I_0 = 1$ ) mask the fact that the REINE intensity ( $I_0$  in the time domain, the total integrated intensity in the frequency domain) decreases markedly under strong coupling. In terms of intensity ratios near/far from rotational resonance, Fig. S9a shows that  $I_0^{\Delta=0 \text{ ppm}}/I_0^{\Delta=4 \text{ ppm}} = 0.28$  and 0.44 respectively for direct and relayed strong coupling. Studying Fig. S9 in combination with Figs S3–8 shows that when it is damped or distorted, the REINE signal under strong coupling (direct or relayed) is always weaker relative to the corresponding signal under weak coupling. At 100 kHz MAS for instance, the REINE curve at  $n = 0$  rotational resonance is damped by a strong zero-frequency component (Fig. S3j), but  $I_0^{\Delta=0 \text{ ppm}}/I_0^{\Delta=4 \text{ ppm}} = 0.08$  only (Fig. S9b).

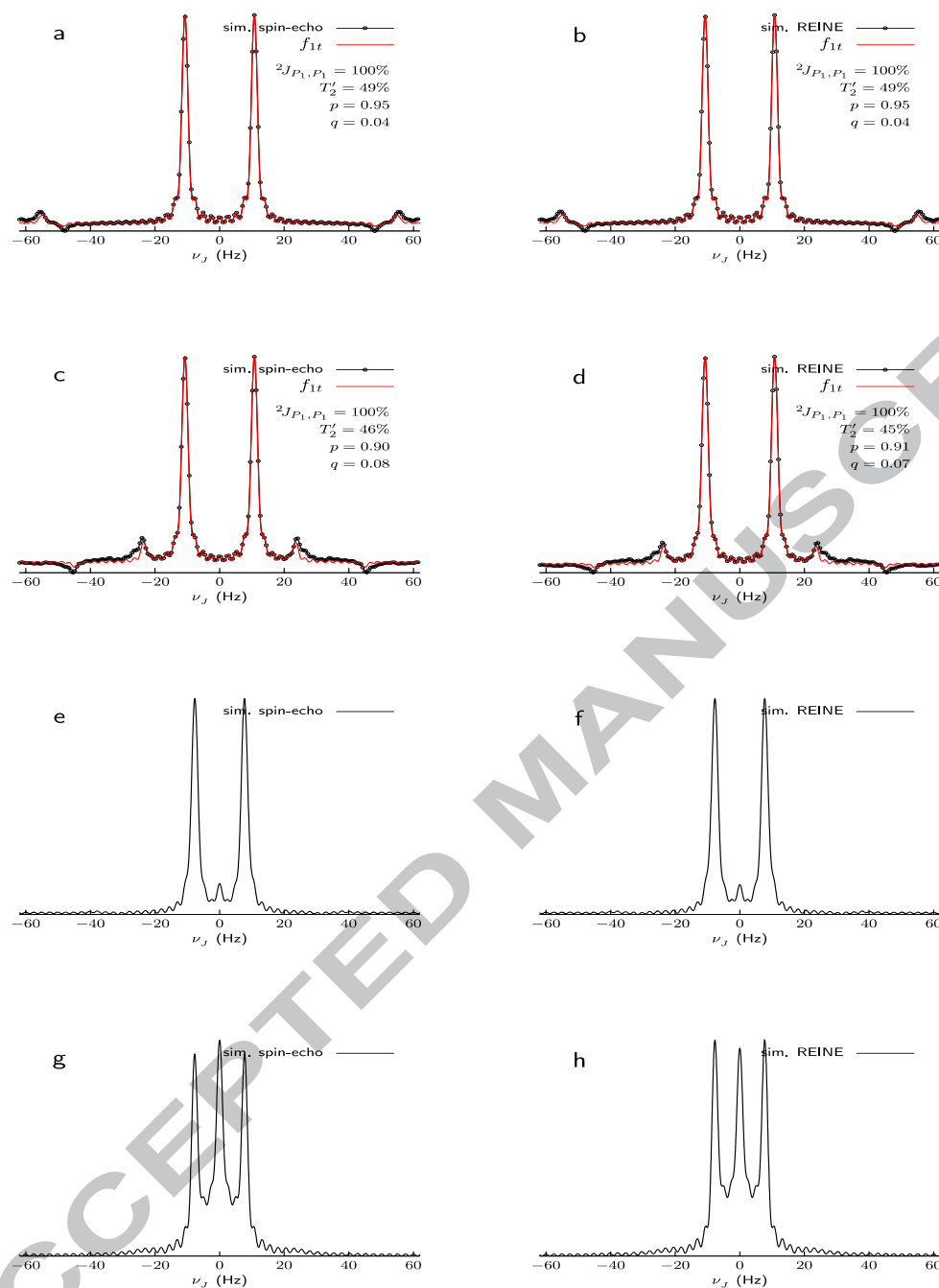
### 3.2. Evidence that spin-echo damping is a strong coupling effect

Fig. 3a–d show that under strong coupling,  $J$  sidebands are observed in both spin-echo and REINE  $J$ -resolved spectra at

$$\nu_j^{\text{band}} = \left[ J \pm (J^2 + \Delta\delta_{\text{iso}}^2)^{1/2} \right] \quad (11)$$

as calculated by Kumar for AB spin systems in solution [2]. Kumar also calculates the intensity of these sidebands:

$$I_j^{\text{band}} = \mp \left( 1 + \frac{J}{(J^2 - \Delta\delta_{\text{iso}}^2)^{1/2}} \right) \frac{J}{(J^2 - \Delta\delta_{\text{iso}}^2)^{1/2}} \quad (12)$$



**Fig. 3.** High resolution  $J$ -resolved spectra of end-of-chain units under (a–d) direct (spinsys2 in Table 1) or (e–h) relayed (spinsys3) strong coupling, close to  $n = 0$  rotational resonance. Simulated  $^{31}\text{P}$  (121.5 MHz) MAS (12.5 kHz) NMR (a, c, e, g) spin-echo and (b, d, f, h) REINE (refocused INADEQUATE spin-echo)  $J$ -resolved spectra of the third spin in three-spin systems at or close to (a–d) direct or (e–h) relayed strong coupling with differences in isotropic chemical shift (a, b)  $\Delta\delta_{\text{iso}}^{2,3} = 0.8$  ppm, (c, d)  $\Delta\delta_{\text{iso}}^{2,3} = 0.4$  ppm (e, f)  $\Delta\delta_{\text{iso}}^{2,3} = 0.4$  ppm and (g, h)  $\Delta\delta_{\text{iso}}^{1,2} = 0.0$  ppm. The red line in parts (a–d) is the Fourier transform of the function  $f_{1t}$  (Table 2), fitted to the corresponding time-domain data set. The optimised fitting parameters (inset) are expressed as a percentage of the corresponding simulated value,  $J^{2,3} = 21.5$  and  $T'_2 = 40$  ms.

At  $\Delta\delta_{\text{iso}} = 0$ , these sidebands coalesce at zero frequency (see Fig. S2c) and the oscillation of the spin-echo curve is damped. (This effect is not observed in solution because the  $J$ -modulation disappears at  $\Delta\delta_{\text{iso}} = 0$ ). In the REINE experiment (Fig. S2d), this zero-frequency component is presumably blocked by the double-quantum filter. There is no direct damping of the spin-echo or REINE data at  $n = 1$  rotational resonance (see Fig. S10) because the sidebands appear at (Eq. 11),

$$\nu_j^{\text{band}} = [J \pm (J^2 - \nu_{\text{MAS}}^2)^{1/2}] \approx \pm \nu_{\text{MAS}} \quad (13)$$

in the frequency dimension, since  $\nu_{\text{MAS}} \gg J$ , and are of negligible intensity:

$$I_j^{\text{band}} \approx \mp \left(1 + \frac{J}{\nu_{\text{MAS}}}\right) \frac{J}{\nu_{\text{MAS}}} \approx 0 \quad (14)$$

These results therefore indicate that direct damping is a strong coupling (i.e. isotropic) effect, made visible by the anisotropic interactions that stabilise the ideal  $J$  modulation.

Regarding the relayed effect, Kumar's analysis of the ABX spin system, of which spinsys3 is a solid-state example, predicts that zero-frequency transitions are detected on the X spin. Similarly, Fig. 3e-h shows that the extra component for spinsys3 always appears at zero-frequency. In this case, relayed damping is also observed at  $n = 1$  rotational resonance (Fig. S10). However, Fig. S11 shows that a  $J$  coupling is required to relay this effect, as no zero-frequency component is observed for spinsys4 (two nearby pairs of  $J$ -coupled spins, one of which has degenerate isotropic chemical shifts). The relayed damping we describe is therefore also a strong coupling effect.

These simulation results suggest that zero-frequency damping should measurably affect spin-echo curves of (linearly or circularly) bonded spin systems in which at least two units are within a few fractions of a ppm of rotational resonance. For REINE data, the appearance of zero-frequency damping is accompanied by a substantial decrease in signal intensity. In practice therefore, this effect should only be detectable in very ordered systems, where it is not masked by the stronger ideal modulations of other groups with similar isotropic chemical shifts.



### 3.3. End-of-chain units: experiments

Fig. 4 shows the  $J$  modulation of the spin-echo intensity at  $-5.3$  ppm ( $P_1$  units, Fig. 4a), and of the REINE intensity at  $[\delta_1, \delta_2] = [-23.1, -5.3]$  ppm ( $P_1$ - $P_2$  units, Fig. 4b) and  $[-5.3, -5.3]$  ppm ( $P_1$ - $P_1$  units, Fig. 4c). The spin-echo modulation is visibly damped (best fit function with  $J$  constrained to be  $> 10$  Hz,  $f_{1a}^0$ ; WoE, 1.00) with respect to the two REINE curves (best fit function,  $f_1^k$ ; WoE, 1.00). There is no evidence of damping in Fig. 4c (WoE for  $f_{1a}^0$ , 0.00) even though the point considered is diagonal. The WoE for  $f_1^k$  is indeed 1.0 across both  $P_1$  REINE peaks. The WoE for  $f_{1a}^0$  across the  $P_1$  peak is 0.98 (0.89–1.00). The models fit the data well, with  $\chi_{\text{red}}^2 = 0.4$  (0.1–1.5), 0.3 (0.2–0.5) and 0.3 (0.1–0.7) respectively for the  $P_1$  spin-echo, and  $P_1$ - $P_2$  and  $P_2$ - $P_2$  REINE peaks. Note that the decay of the REINE modulation curves is best modelled by a mixed Gaussian-Lorentzian function (Eq. 6) [24]. The best fit values (reported as the median value and the range between the 5<sup>th</sup> and 95<sup>th</sup> percentile) for the  $J$  coupling are consistent between the two experiments with  ${}^2J_{P_1, P_2} = 13.7$  (10.6–15.4) Hz (the  $P_2$  notation reflects the overlap between  $P_1$ - $P_1$  and  $P_1$ - $P_2$  signals in the spin-echo data),  ${}^2J_{P_1, P_2} = 16.4$  (15.9–17.8) Hz and  ${}^2J_{P_1, P_1} = 14.7$  (14.1–15.1) Hz, with respective uncertainties of  $\pm 0.6$  (0.2–5.2) Hz,  $\pm 0.2$  (0.1–0.2) Hz and  $\pm 0.2$  (0.1–0.3) Hz. (The median value obtained from the spin-echo data is expected to be slightly lower because the  ${}^2J_{P_1, P_1}$  coupling decreases as the chemical shift increases (becomes less negative) in the direct dimension [8] and the fitted region for the spin-echo data ( $\delta_2 = -0.2$  to  $-7.8$  ppm) extends to higher chemical shifts than those considered for the REINE peaks ( $-1.9$  to  $-13.9$  ppm).)

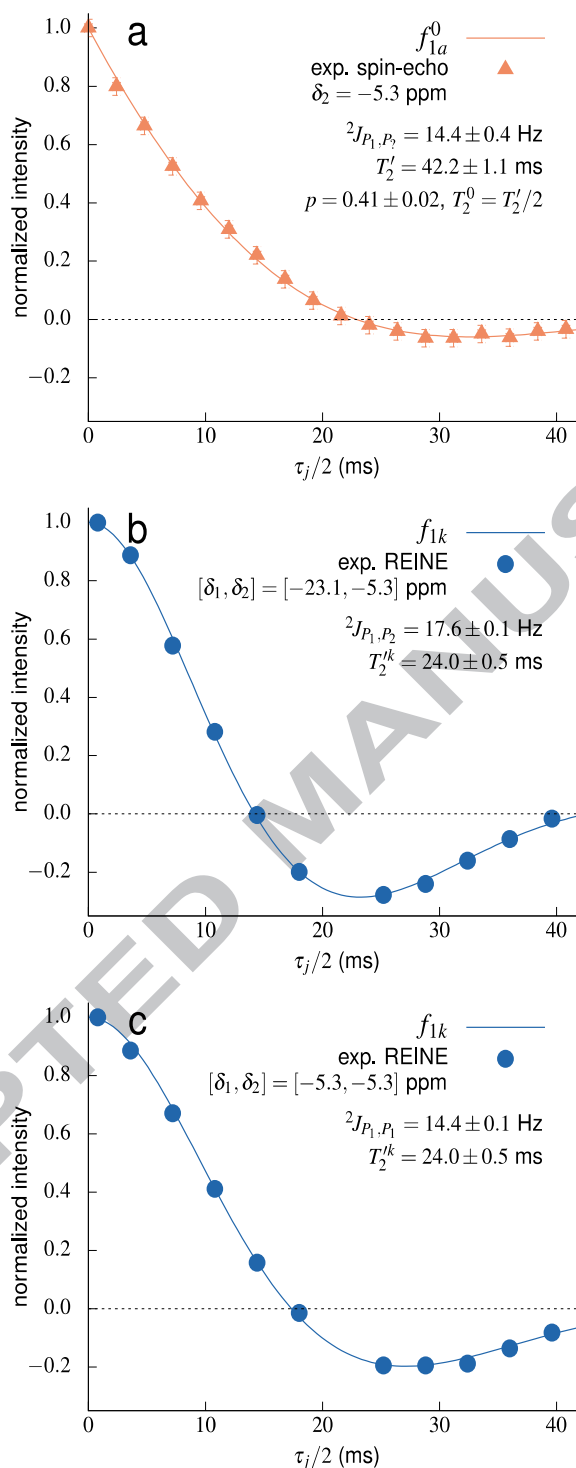


**Fig. 4.** Strong coupling effects in spin-echo and REINE curves from end-of-chain units: experiments.  $^{31}\text{P}$  (121.5 MHz) MAS (12.5 kHz) (a) spin-echo and (b, c) REINE intensities, at the chemical shift coordinates indicated, as a function of the modulating spin-echo delay ( $\tau_j$ ), of  $\text{P}_1$  groups in a cadmium phosphate glass ( $0.575\text{CdO}-0.425\text{P}_2\text{O}_5$ ). The error bars,  $\pm 0.02$ , visible in part (a), are roughly the size of the data points in parts (b) and (c).

### 3.4. Mid-chain units: simulations

Fig. 5 shows spin-echo and REINE curves simulated for spin systems spinsys5–8 (Table 1). As expected, if the observed spin is weakly coupled to its neighbours (spinsys5, Fig. 5a,b), the ideal modulation under two  $J$  couplings is obtained with both experiments, and the data is unambiguously modelled best by  $f_2(\text{WoE}, 1.00)$ .

The curves in Fig. 5c,d are visibly damped with respect to the preceding two, and the spin-echo (Fig. 5c) and REINE (Fig. 5d) data are practically identical. The model that best fits both datasets is again  $f_2(\text{WoE}, 1.00)$ , but with fitted parameters lower than the corresponding simulated values (especially  $T_2'$  and one of the  $J$  couplings). In other words, spin-echo and REINE modulations from mid-chain units are both damped under direct strong coupling. However, the corresponding high resolution  $J$ -resolved spectra (Fig. S12b,c) show multiple extra components rather than a single zero-frequency peak. This is consistent with Kumar's analysis of the ABX spin system [2], namely that 16 transitions are generated for the AB spins with a non-selective  $180^\circ$  pulse, none of which appear at the expected frequencies (i.e.  $J_{A,B}$  or  $J_{B,X}$ ). Since most of these extra components do not appear at zero frequency, our interpretation is that they pass through a double-quantum filter and thus also affect the REINE data.

Spin-echo and REINE modulations from mid-chain units are also damped under relayed strong coupling (Fig. 5e,f), but in this case, the data are best modelled by  $f_{2a}^0(\text{WoE}, 1.00)$ , i.e. with a zero-frequency component. The multiple components that appear in the high-resolution  $J$ -resolved spectra of this spin system (Fig. S12e,f) can therefore be approximated at lower resolution by a single zero-frequency component. However, the values obtained for the  $J$  couplings are incorrect. Finally, Fig. 5g,h show that the expected dual modulation disappears completely for mid-chain units in spin systems with both direct and relayed strong coupling, such that the data are best fit by  $f^0(\text{WoE}, 1.00)$ .

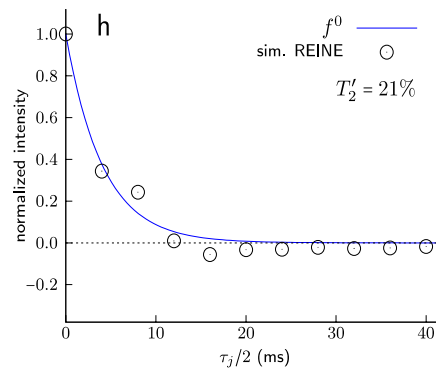
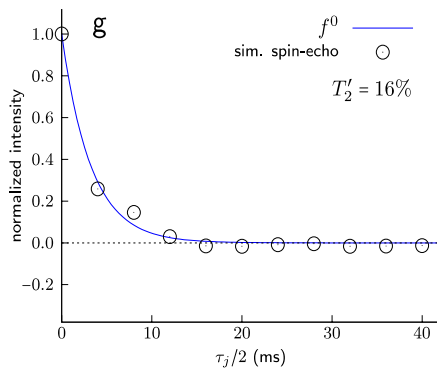
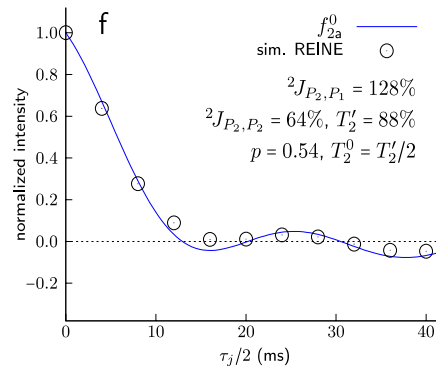
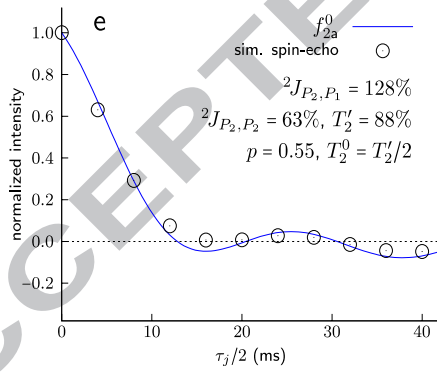
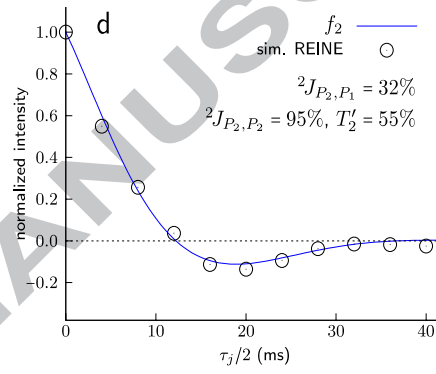
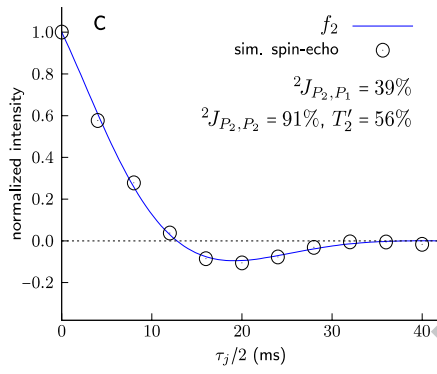
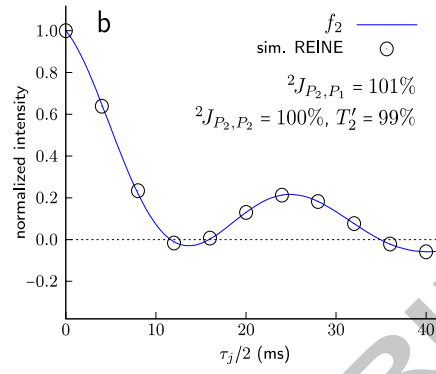
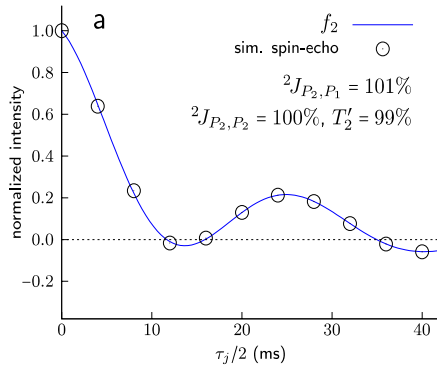


**Fig. 5.** Strong coupling effects in spin-echo and REINE curves from mid-chain units. Simulated  $^{31}\text{P}$  (121.5 MHz) MAS (12.5 kHz) NMR (a, c, e, g) spin-echo and (b, d, f, h) REINE (refocused INADEQUATE spin-echo) intensities as a function of the modulating spin-echo delay ( $\tau_j$ ) of (a–d) the second spin of three-spin systems or (e–h) the third spin of four-spin systems with differences in isotropic chemical shift (a, b)  $\Delta\delta_{\text{iso}}^{1,2} = 4$  ppm (spinsys5 in Table 1), (c, d)  $\Delta\delta_{\text{iso}}^{1,2} = 0.0$  ppm (spinsys6) (e, f)  $\Delta\delta_{\text{iso}}^{1,2} = 0.0$  ppm (spinsys7) and (g, h)  $\Delta\delta_{\text{iso}}^{1,2}$  and  $\Delta\delta_{\text{iso}}^{2,3} = 0.0$  ppm (spinsys8). The optimised fitting parameters (inset) are expressed as a percentage of the corresponding simulated value,  $T_2' = 40$  ms and (a–d)  $J^{1,2} = 21.5$  Hz,  $J^{2,3} = 15.5$  Hz or (e–h)  $J^{1,2} = J^{2,3} = 21.5$  Hz and  $J^{3,4} = 15.5$  Hz.

### 3.5. Mid-chain units: experiments

The experimental data for the  $\text{P}_2$  units in the cadmium phosphate glass all show evidence of damping, as highlighted in Fig. 6a–c for the spin-echo, REINE  $\text{P}_2\text{-P}_1$  and REINE  $\text{P}_2\text{-P}_2$  peaks, respectively. The best model across the entire spin-echo peak is  $f_{2ak}^0$  (WoE, 1.0 (0.79–1.0);  $\chi_{\text{red}}^2$ , 0.5 (0.1–2.3)). The REINE  $\text{P}_2\text{-P}_1$  data are best fit by either  $f_{2ak}^{0k}$  (WoE, 0.78 (0.36–0.93)) or  $f_2^k$  (WoE, 0.20 (0.07–0.62)), the latter with optimal values of  $T_2'^k$  (15.0 (15.0–15.5) ms) substantially lower than those obtained for the  $\text{P}_1\text{-P}_2$  peak (23.0 (22.0–24.0) ms). Nowhere across the  $\text{P}_2\text{-P}_1$  peak does the WoE unambiguously support one function. This is also the case across the  $\text{P}_2\text{-P}_2$  peak, where three models are alternatively best,  $f_2^k$ ,  $f_{2ak}^0$  and  $f_{2ak}^{0k}$ , with respective WoE of 0.48 (0.01–0.77), 0.00 (0.00–0.84) and 0.31 (0.02–0.73). For a small (6% of the total peak area), well-localised subset of the data moreover (roughly the bottom right-hand corner of the peak), the best model is  $f^{0k}$ . The fits are similarly imprecise for both REINE peaks with  $\chi_{\text{red}}^2 = 1.2$  (0.5–2.2) and 0.9 (0.4–2.0) for the  $\text{P}_2\text{-P}_2$  and  $\text{P}_2\text{-P}_1$  peaks, respectively.

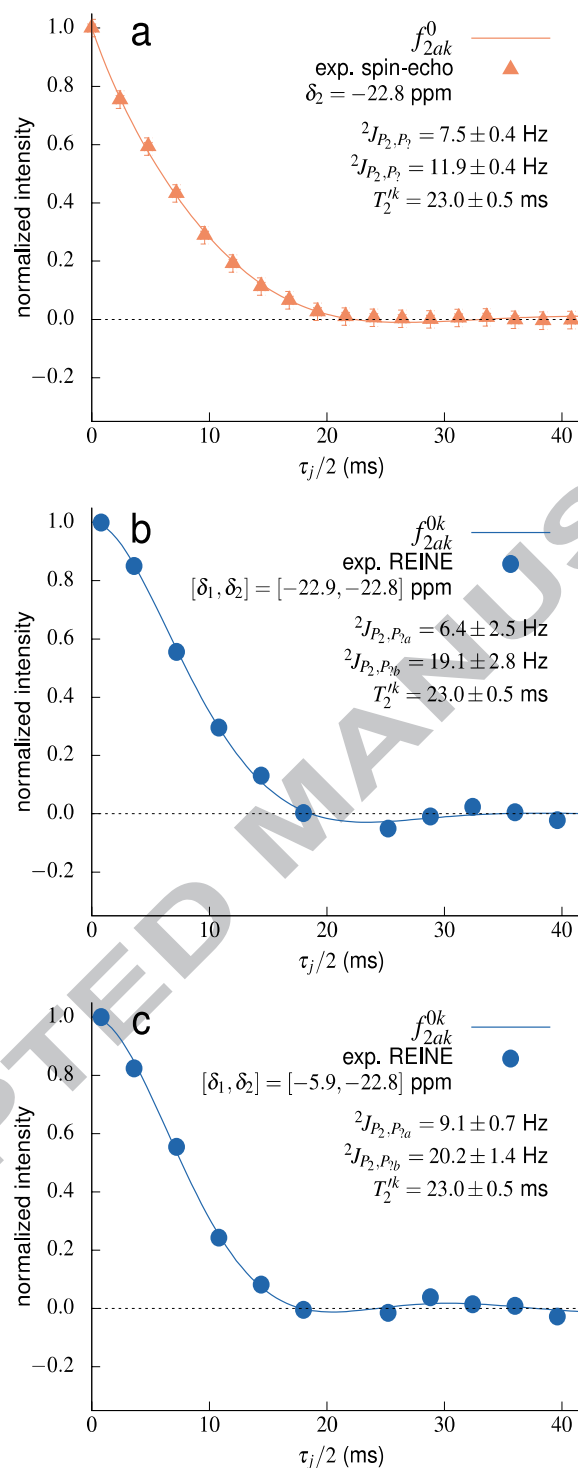


**Fig. 6.** Strong coupling effects in spin-echo and REINE curves from mid-chain units: experiments.  $^{31}\text{P}$  (121.5 MHz) MAS (12.5 kHz) (a) spin-echo and (b, c) REINE intensities, at the chemical shift coordinates indicated, as a function of the modulating spin-echo delay ( $\tau_j$ ), of  $\text{P}_2$  groups in a cadmium phosphate glass ( $0.575\text{CdO}-0.425\text{P}_2\text{O}_5$ ). The error bars,  $\pm 0.02$ , visible in part (a), are roughly the size of the data points in parts (b) and (c).

The fact that all three datasets are damped indicates that a majority of mid-chain units in this glass are either strongly-coupled with their neighbour or are

directly bonded to a strongly coupled pair. The values obtained from the three data sets for the two  $J$  couplings are similar (spin-echo,  $^2J_{P_2,P_{\gamma a}} = 8.0$  (5.1–8.8) Hz and  $^2J_{P_2,P_{\gamma b}} = 12.8$  (11.2–15.4) Hz; REINE  $P_2$ - $P_2$ ,  $^2J_{P_2,P_{\gamma a}} = 9.4$  (6.5–12.2) Hz and  $^2J_{P_2,P_{\gamma b}} = 14.6$  (12.6–21.8) Hz; REINE  $P_2$ - $P_2$ ,  $^2J_{P_2,P_{\gamma a}} = 9.1$  (3.3–11.0) Hz and  $^2J_{P_2,P_{\gamma b}} = 14.9$  (12.6–21.0) Hz). However, since the simulation results for mid-chain units show (section 3.4) that under direct or relayed strong coupling, the extracted  $J$  couplings are unreliable and it would be unwise to interpret these results quantitatively.

#### 4. Discussion

This study emphasises the importance of considering direct and relayed strong coupling effects when attempting to measure  $J$  couplings in disordered solids. For end-of-chain units, provided damping effects are accounted for in the fitting function,  $J$  coupling parameters can be quantified accurately, even under strong coupling. However, the REINE experiment is particularly valuable in this context since as well as offering pair-specific resolution, its echo modulations are not affected by direct damping. Indeed, without prior knowledge of the expected  $J$  coupling strength, the spin-echo data for the  $P_1$  peak of the cadmium phosphate glass are ambiguous as to the presence or not of a zero-frequency component – the fits are of similar quality with a  $J$  coupling roughly half the actual value. Nonetheless, the simpler spin-echo measurements are valuable as a means to validate analyses of REINE data.

The chemical shift correlations measured for this cadmium phosphate glass show that there are as good as none [8]. That is, for a given type of phosphate pair ( $P_1$ - $P_1$ ,  $P_1$ - $P_2$  or  $P_2$ - $P_2$ ), the only factor that governs the likelihood of a given chemical shift combination is the underlying distribution of isotropic shifts. The  $P_1$  spin-echo signal originates mainly therefore from units that are not (directly) strongly coupled, so the damping observed must be a relayed effect. In structural terms, the observation of damping means that many  $P_1$  groups are coupled to strongly coupled  $P_2$  groups, whose nearest neighbour must also therefore be a  $P_2$  unit (ignoring the small proportion of  $P_2$  and  $P_1$  groups with similar isotropic chemical shifts). On this basis, we speculate that  $p$  in  $f_{1a}^0$  (Eq. 4) could be interpreted semi-quantitatively in terms of the average chain length in the glass, stronger damping (lower values of  $p$ ) indicating

a larger proportion of longer chains. It would be interesting to investigate this effect in glasses of different compositions to see if the factor  $p$  varies systematically.

For mid-chain groups under direct or relayed strong coupling, our results show that neither the spin-echo nor REINE curves can be interpreted quantitatively. The fact that the data are fit equally well by several models is not surprising given that all three datasets (spin-echo, REINE  $P_2$ - $P_1$  and REINE  $P_2$ - $P_2$ ) can be (and from all evidence are) affected by both direct and relayed damping. The seemingly weak  $J$  couplings values obtained here and previously [8] from the REINE  $P_2$  peaks are a result of these effects. However, the fact that the different kinds of strong coupling (direct, relayed and direct plus relayed) modify the curves in different ways suggest that a qualitative interpretation is possible in principle. This could then be used to infer chain lengths in a glass; for instance, a  $^{31}\text{P}$  atom manifesting the effects of both direct and relayed strong coupling must belong to a chain at least five units long. The results obtained here for the  $P_2$ - $P_2$  peak suggest that with higher-resolution data, specific areas of the REINE peaks may be assignable to chains of different lengths in this way.

The modulations of five out of the six experimental datasets for the cadmium phosphate glass – those for the four REINE peaks and the  $P_2$  spin-echo peak – are best fit with a mixed Gaussian-Lorentzian decay function (Eq. 6). This function provides unambiguously better fits of the data (WoE, 1.00) than a Lorentzian alone does. Modelling the decay with Eq. 6, the values obtained for the  $J$  couplings are  $^2J_{P_1,P_1} = 14.7 (14.1-15.1) \pm 0.2 (0.1-0.3)$  Hz and  $^2J_{P_1,P_2} = 16.4 (15.9-17.8) \pm 0.2 (0.1-0.2)$  Hz, compared with  $^2J_{P_1,P_1} = 14.0 (13.5-14.7) \pm 0.3 (0.2-0.6)$  Hz and  $^2J_{P_1,P_2} = 16.3 (15.1-18.1) \pm 0.3 (0.2-0.6)$  Hz using a simple exponential [8]. For this dataset in other words, using a mixed Gaussian-Lorentzian decay function improves the accuracy of the fits, but not (within experimental error) the best-fit values of the  $J$  coupling parameter. The fact that this function also improves the fits of REINE data acquired without z-filters [29] indicates that this effect is reproducible and is not due to imperfect z-filters [30]. NMR lineshapes are typically Lorentzian, which is what Eq. 6 (in the time domain) reduces to in the fast modulation limit ( $\Delta\tau_c \gg 1$ ). Here, the best fits were obtained with  $\Delta\tau_c = 1$ , indicating that the spread of transition frequencies is roughly equal to the relaxation rate of the thermal bath. A more detailed investigation of this effect is beyond the scope of this study, but this result suggests



that as well as providing information on the average structure of these glasses, the decay of REINE curves may also shed light on dynamic processes therein.

In summary therefore, although strong coupling complicates the interpretation of solid-state MAS spin-echo and REINE NMR data, this study outlines how the underlying physical parameters can nonetheless be determined or inferred by carefully fitting the modulation curves.

## Acknowledgements

We thank EPSRC for funding the initial stages of this work through grant EP/C000633/1 and Lancaster University for recent support.

## References

- [1] G. Bodenhausen, R. Freeman, G.A. Morris, D.L. Turner, NMR spectra of some simple spin systems studied by two-dimensional fourier transformation of spin echoes, *J. Magn. Reson.* 31 (1978) 75–95. doi:10.1016/0022-2364(78)90172-5.
- [2] A. Kumar, Two-dimensional spin-echo NMR spectroscopy: A general method for calculation of spectra, *J. Magn. Reson.* 30 (1978) 227–249. doi:10.1016/0022-2364(78)90098-7.
- [3] G. Wider, R. Baumann, K. Nagayama, R.R. Ernst, K. Wüthrich, Strong spin-spin coupling in the two-dimensional J-resolved 360-MHz  $^1\text{H}$  NMR spectra of the common amino acids, *J. Magn. Reson.* 42 (1981) 73–87. doi:10.1016/0022-2364(81)90011-1.
- [4] M.J. Thrippleton, R.A.E. Edden, J. Keeler, Suppression of strong coupling artefacts in J-spectra, *J. Magn. Reson.* 174 (2005) 97–109. doi:10.1016/j.jmr.2005.01.012.
- [5] R. Tycko, A “special perspectives” issue: Recent achievements and new directions in biomolecular solid state NMR, *J. Magn. Reson.* 253 (2015) 1. doi:10.1016/j.jmr.2015.02.004.
- [6] R.K. Brow, Review: the structure of simple phosphate glasses, *J. Non-Cryst. Solids.* 263 (2000) 1–28. doi:10.1016/S0022-3093(99)00620-1.
- [7] H. Eckert, Network Former Mixing (NFM) Effects in Ion-Conducting Glasses - Structure/Property Correlations Studied by Modern Solid-State NMR Techniques, *Diffus. Found.* 6 (2016) 144–193. doi:10.4028/www.scientific.net/DF.6.144.
- [8] P. Guerry, M.E. Smith, S.P. Brown,  $^{31}\text{P}$  MAS Refocused INADEQUATE Spin-Echo (REINE) NMR Spectroscopy: Revealing J Coupling and Chemical Shift Two-Dimensional Correlations in Disordered Solids, *J. Am. Chem. Soc.* 131 (2009) 11861–11874. doi:10.1021/ja902238s.
- [9] L. Duma, W.C. Lai, M. Carravetta, L. Emsley, S.P. Brown, M.H. Levitt, Principles of Spin-Echo Modulation by J-Couplings in Magic-Angle-Spinning

- Solid-State NMR, *ChemPhysChem*. 5 (2004) 815–833. doi:10.1002/cphc.200301213.
- [10] A. Lesage, M. Bardet, L. Emsley, Through-Bond Carbon–Carbon Connectivities in Disordered Solids by NMR, *J. Am. Chem. Soc.* 121 (1999) 10987–10993. doi:10.1021/ja992272b.
- [11] F. Fayon, D. Massiot, M.H. Levitt, J.J. Titman, D.H. Gregory, L. Duma, L. Emsley, S.P. Brown, Through-space contributions to two-dimensional double-quantum J correlation NMR spectra of magic-angle-spinning solids, *J. Chem. Phys.* 122 (2005) 194313. doi:10.1063/1.1898219.
- [12] J. Du, Challenges in Molecular Dynamics Simulations of Multicomponent Oxide Glasses, in: C. Massobrio, J. Du, M. Bernasconi, P.S. Salmon (Eds.), *Mol. Dyn. Simul. Disord. Mater.*, Springer International Publishing, Cham, 2015: pp. 157–180. [http://link.springer.com/10.1007/978-3-319-15675-0\\_7](http://link.springer.com/10.1007/978-3-319-15675-0_7).
- [13] T.F. Green, J.R. Yates, Relativistic nuclear magnetic resonance J-coupling with ultrasoft pseudopotentials and the zeroth-order regular approximation, *J. Chem. Phys.* 140 (2014) 234106.
- [14] M.M. Maricq, J.S. Waugh, NMR in rotating solids, *J. Chem. Phys.* 70 (1979) 3300–3316. doi:10.1063/1.437915.
- [15] A. Kubo, A. Root, C.A. McDowell, Two dimensional  $^{31}\text{P}$  nuclear magnetic resonance coherence transfer experiments under magic-angle sample spinning, *J. Chem. Phys.* 93 (1990) 5462–5472. doi:10.1063/1.459615.
- [16] R. Challoner, T. Nakai, C.A. McDowell, J coupling in chemically equivalent spin pairs as studied by solid-state nuclear magnetic resonance, *J. Chem. Phys.* 94 (1991) 7038–7045. doi:10.1063/1.460237.
- [17] M. Bak, J.T. Rasmussen, N.C. Nielsen, SIMPSON: A General Simulation Program for Solid-State NMR Spectroscopy, *J. Magn. Reson.* 147 (2000) 296–330. doi:10.1006/jmre.2000.2179.
- [18] P. Guerry, S.P. Brown, M.E. Smith, Dataset for “Strong-coupling induced damping of spin-echo modulations in magic-angle-spinning NMR: implications for J coupling measurements in disordered solids,” (2017).
- [19] J.K. Christie, R.I. Ainsworth, N.H. de Leeuw, Ab initio molecular dynamics simulations of structural changes associated with the incorporation of fluorine in bioactive phosphate glasses, *Biomaterials*. 35 (2014) 6164–6171. doi:10.1016/j.biomaterials.2014.04.032.
- [20] J.T. Hoggins, J.S. Swinnea, H. Steinfink, Crystal structure of  $\text{Fe}_2\text{P}_2\text{O}_7$ , *J. Solid State Chem.* 47 (1983) 278–283. doi:10.1016/0022-4596(83)90019-1.
- [21] J.-J. Liang, R.T. Cygan, T.M. Alam, Molecular dynamics simulation of the structure and properties of lithium phosphate glasses, *J. Non-Cryst. Solids*. 263–264 (2000) 167–179. doi:10.1016/S0022-3093(99)00632-8.
- [22] S.T. Norberg, G. Svensson, J. Albertsson, A  $\text{TiP}_2\text{O}_7$  superstructure, *Acta Crystallogr. C*. 57 (2001) 225–227. doi:10.1107/S0108270100018709.
- [23] R. Hussin, D. Holland, R. Dupree, A MAS NMR structural study of cadmium phosphate glasses, *J. Non-Cryst. Solids*. 298 (2002) 32–42. doi:10.1016/S0022-3093(01)01049-3.
- [24] R. Kubo, A Stochastic Theory of Line Shape, *Adv. Chem. Phys.* 15 (1969) 101–127.
- [25] D.V. Matyushov, Kubo’s Line Shape Function for a Linear-Quadratic Chromophore–Solvent Coupling, *J. Phys. Chem. B*. 119 (2015) 9006–9008. doi:10.1021/jp5081059.

- [26] H. Akaike, Likelihood of a model and information criteria, *J. Econom.* 16 (1981) 3–14. doi:10.1016/0304-4076(81)90071-3.
- [27] K.P. Burnham, D.R. Anderson, eds., *Model Selection and Multimodel Inference*, Springer New York, New York, NY, 2004. <http://link.springer.com/10.1007/b97636> (accessed January 24, 2017).
- [28] K.P. Burnham, Multimodel Inference: Understanding AIC and BIC in Model Selection, *Sociol. Methods Res.* 33 (2004) 261–304. doi:10.1177/0049124104268644.
- [29] P. Guerry, *New solid-state NMR approaches to the structural characterisation of phosphate glasses*, University of Warwick, 2008. <http://ethos.bl.uk/OrderDetails.do?uin=uk.bl.ethos.495018> (accessed January 25, 2017).
- [30] P. Guerry, S.P. Brown, M.E. Smith, Improving the sensitivity of J coupling measurements in solids with application to disordered materials, *AIP Adv.* 6 (2016) 55008. doi:10.1063/1.4948965.

**Highlights**

- Strong coupling effects are shown to affect solid-state NMR echo curves.
- REINE data are less affected than spin-echo data.
- A method is proposed to interpret the modified echo curves.
- Applications for the study of disordered solids are envisaged.

**Graphical abstract**